
Visionary: The World Model Carrier Built on WebGPU-Powered Gaussian Splatting Platform

Yuning Gong^{1,2,*} Yifei Liu¹ Yifan Zhan³ Muyao Niu³ Xueying Li⁴
Yuanjun Liao^{1,2} Jiaming Chen² Yuanyuan Gao^{1,5} Jiaqi Chen^{1,5} Minming Chen¹
Li Zhou¹ Yuning Zhang¹ Wei Wang¹ Xiaoqing Hou¹ Huaxi Huang¹
Shixiang Tang¹ Le Ma¹ Dingwen Zhang⁵ Xue Yang⁴ Junchi Yan^{1,4}
Yanchi Zhang² Yinqiang Zheng³ Xiao Sun¹ Zhihang Zhong^{1,✉}

¹Shanghai AI Laboratory ²Sichuan University ³The University of Tokyo
⁴Shanghai Jiao Tong University ⁵Northwestern Polytechnical University

Code: <https://github.com/Visionary-Laboratory/visionary>

Abstract

Neural rendering, particularly 3D Gaussian Splatting (3DGS), has evolved rapidly and become a key component for building world models. However, existing viewer solutions remain fragmented, heavy, or constrained by legacy pipelines, resulting in high deployment friction and limited support for dynamic content and generative models. In this work, we present **Visionary**, an open, web-native platform for real-time various Gaussian Splatting and meshes rendering. Built on an efficient WebGPU renderer with per-frame ONNX inference, Visionary enables dynamic neural processing while maintaining a lightweight, “click-to-run” browser experience. It introduces a standardized Gaussian Generator contract, which not only supports standard 3DGS rendering but also allows plug-and-play algorithms to generate or update Gaussians each frame. Such inference also enables us to apply feedforward generative post-processing. The platform further offers a plug in `three.js` library with a concise TypeScript API for seamless integration into existing web applications. Experiments show that, under identical 3DGS assets, Visionary achieves superior rendering efficiency compared to current Web viewers due to GPU-based primitive sorting. It already supports multiple variants, including MLP-based 3DGS, 4DGS, neural avatars, and style transformation or enhancement networks. By unifying inference and rendering directly in the browser, Visionary significantly lowers the barrier to reproduction, comparison, and deployment of 3DGS-family methods, serving as a unified *World Model Carrier* for both reconstructive and generative paradigms.

1 Introduction

Neural rendering, particularly 3D Gaussian Splatting (3DGS) [34], has advanced rapidly in recent years and has become a key building block for world models [25]. Its efficiency and visual quality enable interactive, real-time 3D experiences that were previously impractical. However, a critical gap remains in deployment: while research focuses on training larger and more sophisticated models, the capability to distribute and execute these dynamic, and heterogeneous representations on consumer

*This work was initiated during an internship at the Shanghai AI Laboratory. ✉ denotes the corresponding author (zhongzhihang@pjlab.org.cn).

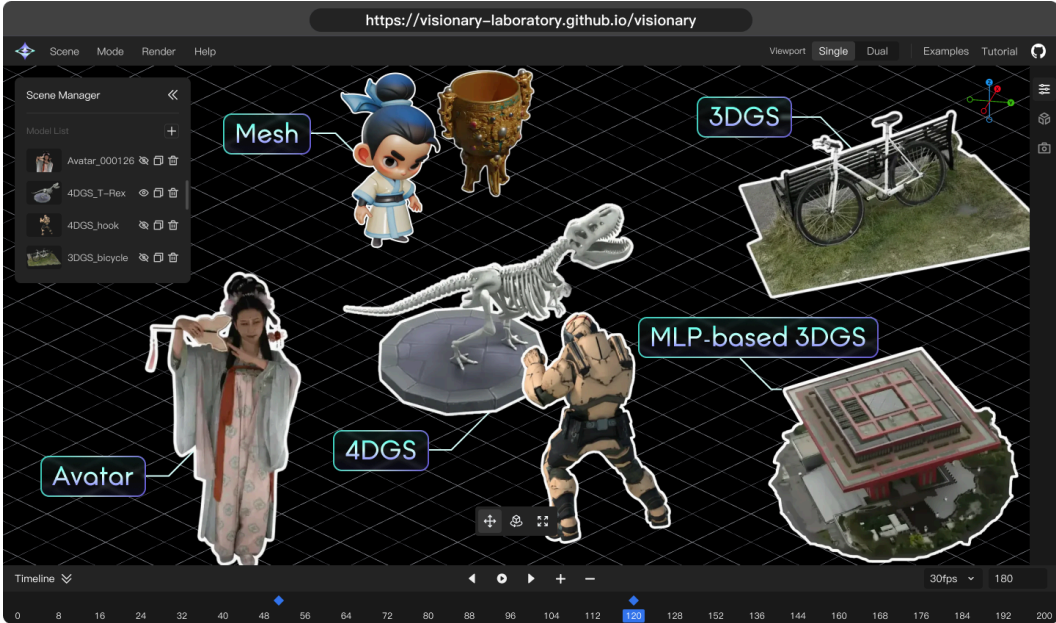


Figure 1: **Visionary as a Universal Runtime.** Visionary’s core system is packaged as a `three.js` plug-in for seamless extension and integration. As a demonstration, we present a lightweight web-based editor that runs directly in the browser: by simply visiting a URL, users can leverage local computing resources through WebGPU to efficiently and simultaneously render multiple heterogeneous 3D/4D Gaussian assets, while maintaining full compatibility with traditional mesh-based rendering pipelines.

devices has lagged behind. Currently, there is an urgent need for a lightweight, flexible, and unified platform that can support the ever-expanding 3DGS ecosystem in a practical and accessible manner.

Existing systems suffer from significant deployment friction and limited extensibility. On the desktop, client-based frameworks such as SIBR [34] and engine-bound plug-ins for Unity, Blender, or Unreal Engine rely on heavy native stacks, including tightly coupled tool-chains and driver dependencies. While performant, these systems are difficult to configure, cumbersome to share, and poorly suited for rapid experimentation or integration of third-party algorithms. On the web, viewers such as SparkJS, SuperSplat, and GaussianSplats3D are constrained by legacy WebGL pipelines, which restrict support for dynamic scenes, animatable avatars, and the integration of generative models. As a result, many demonstrations rely on precomputed Gaussians or server-side inference, reducing both interactivity and reproducibility.

Despite these limitations, web-based platforms remain highly attractive due to their accessibility and platform independence. This motivates a core challenge: how to design a browser-based system that can (i) support heterogeneous 3DGS algorithms without requiring users to re-engineer rendering pipelines or write low-level shader code, and (ii) tightly couple per-frame inference with high-throughput GPU rendering while maintaining real-time performance within a browser environment.

To address these challenges, we propose **Visionary**, a web-native *World Model Carrier* built on a WebGPU-based Gaussian Splatting platform. Visionary removes native dependency overhead by leveraging WebGPU as a unified compute and graphics backend, and standardizes algorithm integration through ONNX-based per-frame inference. At its core is the Gaussian Generator contract, defined by a rigorous ONNX I/O schema and metadata, which specifies how algorithms generate or update Gaussian attributes, including position, scale, orientation, and color. Any 3DGS-family method can be loaded as a plug-in, executed directly in the browser, and rendered efficiently without modification to the underlying runtime.

Built on a fully browser-resident pipeline, Visionary unifies compute and rendering to support dynamic 3DGS workflows entirely on the client side. The current platform supports classic 3DGS, MLP-based 3DGS [51], neural avatars [30, 94, 64], and 4DGS [88] for dynamic scenes, along with

generative post-processing networks [68, 80, 11]. We further offer a `three.js` plug-in and exposed through a concise TypeScript API, enabling seamless integration with existing web applications. Across representative static and dynamic scenes, Visionary sustains real-time interactive performance and demonstrates substantial improvements in frame time, dynamic update latency, and scalability compared to existing web-based renderers.

The contributions of this work are as follows:

- Visionary, a web-native *World Model Carrier* that unifies per-frame ONNX inference with a WebGPU-based Gaussian Splatting renderer and generative post-processing, enabling fully dynamic 3D neural rendering in the browser.
- The Gaussian Generator contract, a standardized ONNX I/O and metadata interface that enables seamless plug-and-play integration of customized 3DGS algorithms without modifying the rendering pipeline.
- A reference WebGPU implementation and `three.js` API, providing superior efficiency over WebGL-based viewers and straightforward integration into existing web engines for research and application development.

2 Related Works

2.1 3D Gaussian Splatting

Neural Radiance Fields (NeRF) [56, 6, 62, 19, 57, 42, 93] ignited the modern wave of neural rendering and corresponding down-stream applications [61, 78, 13]. However, volumetric NeRF rendering remains computationally expensive due to dense ray marching and repeated neural field evaluations. To address this inefficiency, 3D Gaussian Splatting [34] was introduced as an explicit, point-based alternative, which offer comparative render quality and extreme fast rendering speed.

Building on the success of 3DGS, a rich ecosystem of extensions rapidly emerged. Methods such as 2DGS [98], PGSR [10], GOF [92], and RaDe-GS [96] provide more accurate depth rendering and establish tighter connections between Gaussian primitives and mesh-based representations. Structured 3D Gaussian like Scaffold-GS [51] and Octree-GS [65] further improve rendering quality and efficiency through structured anchors and neural decoding. While 3DGS is significantly more efficient than NeRF, scaling to city-level environments exposes new limitations in efficient training. Large-scale systems, including CityGaussian [48], VastGaussian [45], Hier-GS [35], and CityGS-X [24] propose specialized pipelines for training and rendering in expansive outdoor scenes. Concurrently, researchers have observed that Gaussian primitives often become overly fragmented and redundant, motivating a line of work on compression and pruning, such as LightGaussian [18], Compact-3DGS [36], and MaskGaussian [49]. Recently, some studies [91, 23] have begun exploring the use of hardware rasterization techniques to accelerate the rendering process of 3DGS. Beyond static scenes, dynamic extensions have emerged as well, including 4D Gaussian Splatting [88, 79, 5, 15, 31, 41, 50, 73, 90, 14], and a series of work focusing on avatar reconstruction and animation [30, 63, 43, 59, 64, 84, 95, 58]. More recently, a parallel thread of feedforward Gaussian reconstruction methods [9, 12, 37, 33], to bypass iterative optimization altogether and enable real-time reconstruction.

Overall, the 3DGS family has expanded rapidly, producing diverse representations, training paradigms, and rendering pipelines. This diversity highlights the need for a flexible, unified viewer architecture capable of visualizing, comparing, and mixing different Gaussian-based representations for research and content creation.

2.2 3DGS Viewers and Plugins

Effective visualization is crucial for the evaluation and deployment of neural rendering methods. Research-oriented frameworks typically employ desktop-based architectures to achieve high-performance rendering. The official SIBR viewer [34] relies on C++/CUDA to ensure efficiency but remains a standalone research tool. Similarly, Splatfacto, included in the Nerfstudio [74] framework, provides a browser-based interface for effective training monitoring. Nevertheless, as a client-server system coupled with the training engine, it necessitates a heavy local Python/CUDA backend and the original input data for initialization. To leverage mature development ecosystems,

plugins for game engines and content creation tools including Unity, Unreal Engine, and Blender were developed. These plugins allow 3DGS to interact with engine-specific features such as physics and lighting. However, both standalone viewers and engine-based plugins suffer from significant deployment friction. They typically require heavy installation stacks, specific GPU drivers (*e.g.*, CUDA), and in the case of plugins, strict compatibility with specific engine versions. Such tight coupling and hardware dependency make these systems ill-suited for rapid sharing, lightweight reproduction, or cross-platform accessibility.

On the other hand, web-based viewers such as GaussianSplats3D, SuperSplat, and SparkJS allow users to view static scenes directly in a browser without software installation. However, most existing web viewers rely on legacy WebGL pipelines. This dependence imposes severe performance bottlenecks, often necessitating CPU-based primitive sorting, which limits scalability for large scenes. Furthermore, the lack of flexible compute shader support in WebGL restricts these viewers to static assets, preventing the integration of dynamic Gaussian decoding or complex generative post-processing pipelines on the client side.

Compared with other desktop or web based solutions, our platform Visionary offers web-native accessibility and real-time WebGPU performance, while additionally supporting advanced 3DGS variants and generative models through a flexible ONNX interface.

2.3 World Models and Interactive Generative Video

A world model aims to internalize the governing laws of a physical environment, learning to predict future states based on current observations and actions. This capability holds transformative potential spanning a wide range of verticals, promising to enable high-fidelity industrial digital twins, immersive entertainment and even personalized interactive education. To facilitate scalability, the dominant paradigm of world models bypasses explicit 3D reconstruction, instead learning auto-regressively from vast video data to simulate the “world” as a sequence of 2D latent frames, manifested as Interactive Generative Video (IGV). Prominent general-purpose foundation models, such as Genie 3, V-JEPA 2 [4], and Cosmos 2.5 [2], exemplify this approach, demonstrating remarkable capabilities in synthesizing diverse visual dynamics. This methodology has seen rapid adoption across specific domains as well, ranging from autonomous driving [76, 21, 40, 77, 100, 22, 28, 97, 70, 66] and embodied robotic manipulation [1, 102, 72, 52, 101] to open-world gaming agents [82, 16, 27, 3] and science [99, 89, 87]. However, lacking explicit spatial understanding, these models suffer from inherent 3D inconsistency, frequently exhibiting “geometric hallucinations” and failing to maintain consistent object identity. Consequently, the generated “worlds” often lack the physical realism and long-horizon stability essential for rigorous simulation.

Leveraging advancements in feed-forward Gaussian splatting [9, 12, 33] and VGGT [75], recent research [67, 53, 81, 38] integrates 3D priors into the latent state space to enforce physical plausibility. Unlike transient 2D features, explicit 3D intermediate states ensure superior multi-view consistency, allowing the “camera” to move freely without breaking the scene’s illusion while providing a robust global memory bank. However, realizing the full potential of such high-fidelity representations requires accessible visualization tooling. Our platform addresses this infrastructural need by offering a standardized ONNX-based pipeline for the real-time inspection of explicit 3D states. Furthermore, its inherent compatibility with IGV workflows makes it an ideal testbed for developing next-generation, physics-aware World Models.

3 Pipeline

3.1 Overview

The overall design of Visionary follows three guiding principles. **Web-native first:** all components run directly in the browser via WebGPU, enabling zero-install sharing, on-device inference for privacy, and consistent behavior across operating systems. **Contract-driven extensibility:** algorithms are exported to ONNX, while the runtime handles scheduling, memory management, and rendering, eliminating the need for per-algorithm code branches. **Real-time coupling:** inference and rendering are executed within a single frame budget, enabling fast interaction. The overall pipeline is illustrated in Figure 2. We first review the definition of 3DGS in Section 3.2. In Section 3.3, we present the Gaussian Generator contract built on ONNX and demonstrate several representative 3DGS variants.

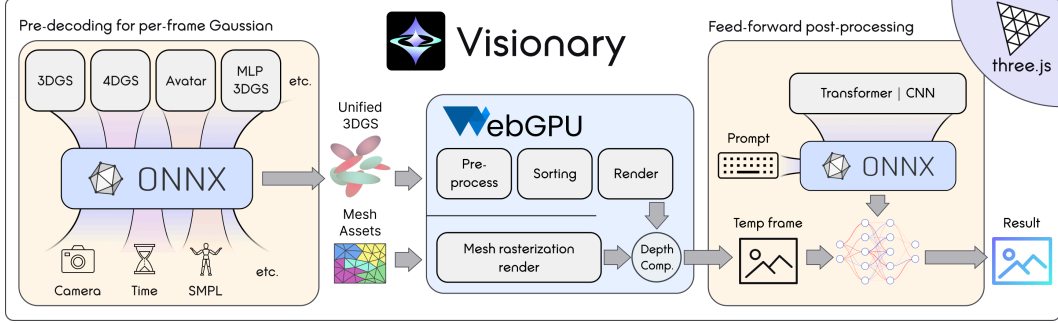


Figure 2: **Pipeline of Visionary.** Visionary first performs pre-decoding through ONNX to support diverse 3DGS variants. The generated Gaussians are then combined with optional mesh assets and passed into a WebGPU-based hybrid rendering pipeline, where depth-aware composition produces the final image. In the post-processing stage, ONNX-based generative models can be optionally applied for tasks such as stylization and enhancement, yielding the final output.

We then describe the WebGPU-based rendering pipeline for hybrid 3DGS and mesh visualization in Section 3.4. Finally, in Section 3.5, we introduce how generative models can also be integrated through ONNX for post-processing.

3.2 Definition of 3DGS

Gaussian Splatting represents a scene as a set of N anisotropic 3D Gaussian primitives: $\mathcal{G} = \{G_i\}_{i=1}^N$, where each Gaussian G_i is defined by a mean position $\mu_i \in \mathbb{R}^3$, a covariance matrix $\Sigma_i \in \mathbb{R}^{3 \times 3}$, which is derived from a scale $s_i \in \mathbb{R}^3$ and a rotation quaternion $r_i \in \mathbb{R}^4$, an opacity $\alpha_i \in (0, 1)$, and a view-independent color $\mathbf{c}_i \in [0, 1]^3$ encoded by spherical harmonics.

For a camera with projection operator $\Pi(\cdot)$, each 3D Gaussian is projected to a 2D elliptical Gaussian

$$\mathbf{x}_i = \Pi(\mu_i), \quad \mathbf{S}_i = \mathbf{J}_i \Sigma_i \mathbf{J}_i^\top, \quad (1)$$

where \mathbf{J}_i denotes the Jacobian of Π at μ_i . Given a pixel location \mathbf{x} , its contribution from Gaussian i is modeled as

$$w_i(\mathbf{x}) = \alpha_i \exp\left(-\frac{1}{2}(\mathbf{x} - \mathbf{x}_i)^\top \mathbf{S}_i^{-1}(\mathbf{x} - \mathbf{x}_i)\right). \quad (2)$$

Following front-to-back alpha compositing, the rendered color at pixel \mathbf{x} is computed as

$$\mathbf{C}(\mathbf{x}) = \sum_{i=1}^N \left(w_i(\mathbf{x}) \prod_{j < i} (1 - w_j(\mathbf{x})) \right) \mathbf{c}_i, \quad (3)$$

where Gaussians are sorted by depth w.r.t. the camera. This splatting formulation enables differentiable rendering and efficient optimization of all Gaussian parameters through gradient descent.

3.3 ONNX-based Gaussian Pre-decoding

3DGS has many variants, each adopting different algorithms to produce the final rendering. For example, MLP-based 3DGS [51] decodes Gaussians from anchors according to a give camera view and then rasterizes the decoded Gaussians, while 4DGS [79] computes a deformation field based on a timestamp and then rasterizes the deformed Gaussians. To avoid modifying the renderer for each existing or newly proposed method, we decided to split the rendering logic into two parts: a method-specific pre-decoding stage and a unified renderer.

To support heterogeneous 3DGS-family methods without modifying the renderer, Visionary adopts an ONNX-based *pre-decoding* stage, where each algorithm is exported as a plugin that generates or updates Gaussian attributes every frame. We formalize this interface as the **Gaussian Generator** contract, specified by a fixed set of ONNX I/O tensors and accompanying metadata, enabling contract-driven extensibility. ONNX (Open Neural Network Exchange) serves as an open standard for

machine learning interoperability, defining a common computation graph representation independent of specific frameworks. By leveraging this ecosystem, models trained in diverse environments (*e.g.*, PyTorch or TensorFlow) can be unified and deployed seamlessly across different backends.

Contract I/O. At runtime, the client provides lightweight per-frame inputs (*e.g.*, frame index, control signals or camera). The ONNX graph outputs a variable number of Gaussians \mathcal{G}_t in a packed layout (position, opacity, upper-covariance, and appearance), along with model-level metadata such as number of points and data types (FP32/FP16). The renderer consumes these outputs directly as storage buffers for the WebGPU pipeline.

Why pre-decoding? By encapsulating method-specific neural decoding and deformation logic inside ONNX, Visionary avoids per-method shader branches and heavy native dependencies. For example, in avatar animation, the skeletal forward kinematics and per-Gaussian deformation can be exported into the ONNX graph, so the browser only feeds compact pose parameters while receiving deformed Gaussians ready for rasterization.

Representative variants. In the following subsections, we instantiate this contract for multiple families, including MLP-based 3DGS, 4DGS, and neural avatars, demonstrating that diverse representations can be unified under the same pre-decoding \rightarrow rendering pipeline.

Deployment-oriented graph optimizations. Beyond unifying heterogeneous variants under a single ONNX pre-decoding contract, we introduce two practical optimizations to improve real-time robustness on ONNX Runtime WebGPU.

(i) Enabling capture_graph. For per-frame generators with repetitive execution patterns, we revise the runtime scheduling and I/O binding logic to make the inference path compatible with WebGPU graph capture. Concretely, we keep the session and bindings stable across frames (with an optional warm-up run) so that the runtime can reuse the captured execution graph, reducing JavaScript-side dispatch overhead and stabilizing frame time.

(ii) Post-export rewriting for large Concat/Split patterns. In some exported models, a large number of per-slot tensors are concatenated or split in a single operator (*e.g.*, one-shot Concat over many slots, followed by Split for downstream consumers). Such patterns can be fragile under current WebGPU limits. We therefore apply a lightweight post-processing pass on the exported ONNX graph to partition these operations into smaller, equivalent chunks (*e.g.*, chunked concat/slice-based splits), producing a WebGPU-friendly graph while preserving the same packed output layout required by the Gaussian Generator contract.

3.3.1 Support for MLP-based 3DGS

MLP-based 3DGS like Scaffold-GS [51] and Octree-GS [65] have been proposed to use MLP to decode Gaussians from anchors that store shared features of nearby Gaussians, which offers better visual quality and reduced storage. We leverage Scaffold-GS [51] to demonstrate the methodology for exporting such representation into the ONNX format and integrating into our platform. Instead of directly reconstructing Gaussians from sparse SfM points, these methods first extract a sparse voxel grid and place anchors at the centers of occupied voxels. Each anchor is associated with a feature vector f_i , which is fed into a multi-layer perceptron (MLP) to generate neural Gaussian parameters:

$$\{(\mu_j, \Sigma_j, c_j, \alpha_j) \mid j \in \mathcal{M}\} = \{\text{MLP}_\theta(f_i, d_{\text{view}}) \mid i \in \mathcal{N}\}, \quad (4)$$

where θ denotes the learnable MLP weights, and μ_j , Σ_j , c_j , and α_j represent the mean, covariance, color, and opacity of the j -th neural Gaussian generated from the i -th anchor under viewing direction d_{view} . These neural Gaussians are then rasterized using the standard 3DGS formulation.

While MLP-based 3DGS methods exhibit strong rendering flexibility, Eq. Equation (4) reveals a key challenge: the neural Gaussian parameters must be re-generated for every frame, making real-time online visualization difficult. To the best of our knowledge, no existing system provides an interactive, in-browser viewer for such dynamically generated Gaussians.

To address this limitation, we integrate the MLP-based 3DGS pipeline with ONNX Runtime WebGPU and enable efficient, browser-side visualization. Specifically, we export the trained MLP, along with the anchor positions, scales, and feature vectors, into a static ONNX compute graph. This design allows

the viewer to compute neural Gaussian parameters on-the-fly for arbitrary camera poses, enabling fast, real-time visualization directly in the browser.

3.3.2 Support for 4DGS

To address the challenge of reconstructing and rendering dynamic scenes, mainstream 4D Gaussians approaches typically circumvent the prohibitive storage overhead of storing Gaussian parameters for every individual frame. Instead, their modeling often combines a **canonical space** with a **neural deformable field**. We leverage 4D Gaussians [79] as a representative case to demonstrate the methodology for exporting such deformable fields into the ONNX format.

Specifically, 4D Gaussians employs an efficient HexPlane representation (akin to K-Planes [71]) for spatiotemporal feature encoding. Rather than relying on computationally intensive implicit MLP to model the deformation field, this method factorizes the 4D manifold into six orthogonal 2D feature planes (*i.e.*, $P_{xy}, P_{xz}, P_{yz}, P_{xt}, P_{yt}, P_{zt}$). For each Gaussian primitive in the canonical space, its coordinates and current timestamp (x, y, z, t) are projected onto these multi-resolution planes to retrieve corresponding feature vectors via bilinear interpolation. These features are subsequently concatenated and fed into a lightweight multi-head MLP decoder φ to predict the deformation attributes, specifically position offsets $(\Delta x, \Delta y, \Delta z)$, rotation corrections Δr , and scaling variations Δs . This process effectively transforms the static canonical Gaussians into their time-dependent states for real-time rendering.

To integrate 4D Gaussians [79] into our platform, we established a comprehensive training-to-export pipeline. We developed a custom wrapper that encapsulates the deformation network, comprising multi-resolution feature grids P and the MLP decoder φ , into a standalone `torch.nn.Module`. This design effectively decouples the inference logic from training-specific rasterization operators, ensuring compatibility with standard ONNX runtimes. Notably, our exported model embeds the canonical Gaussian attributes directly as internal constant tensors (Initializers), rather than requiring external inputs. Consequently, the model accepts a scalar timestamp t as the sole input to query the HexPlane and output deformation residuals. This self-contained architecture obviates the need for external geometry files (*e.g.*, PLY), streamlining the web client’s reconstruction workflow via a unified ONNX model.

3.3.3 Support for Animatable Human Avatar

Our platform supports a broad class of animatable human avatar methods that utilize a **canonical space** formulation decoupled from the deformation logic. In this paradigm, the scene is represented by a set of static canonical 3D Gaussians in a neutral pose (*e.g.*, T-pose), which are dynamically warped to the observation space driven by a parametric body model (*e.g.*, SMPL-X [60]).

Let the canonical representation be denoted as $\mathcal{G}_{can} = \{\hat{G}_i\}_{i=1}^N$, where each primitive \hat{G}_i typically contains a mean position $\hat{\mu}_i$, a covariance $\hat{\Sigma}_i$, and learnable skinning weights $\mathcal{W}_i = \{w_{i,k}\}_{k=1}^K$ associated with K skeletal joints. The deformation is generally modeled via Linear Blend Skinning (LBS). Given the body pose parameters θ and shape parameters β for a specific frame, the parametric model defines a global transformation matrix $\mathbf{M}_k(\theta, \beta) \in SE(3)$ for each joint k . The local transformation \mathbf{T}_i for the i -th Gaussian is computed by aggregating these joint transformations:

$$\mathbf{T}_i(\theta, \beta) = \sum_{k=1}^K w_{i,k} \mathbf{M}_k(\theta, \beta) = \begin{bmatrix} \mathbf{R}_i & \mathbf{t}_i \\ \mathbf{0} & 1 \end{bmatrix}, \quad (5)$$

where \mathbf{R}_i and \mathbf{t}_i represent the blended rotation and translation, respectively. Consequently, the deformed attributes for the live frame are updated as:

$$\begin{aligned} \mu_i &= \mathbf{T}_i \cdot \hat{\mu}_i, \\ \Sigma_i &= \mathbf{R}_i \hat{\Sigma}_i \mathbf{R}_i^\top. \end{aligned} \quad (6)$$

This formulation allows the renderer to handle diverse avatar methods that adhere to the canonical-deformation schema.

As a representative implementation of this paradigm, we integrate LHM [64] into our ONNX-based pipeline. LHM learns a high-fidelity canonical representation driven by SMPL-X. To enable web-based rendering, we export the deformation logic into a specialized ONNX graph. In this setup, the

Algorithm Pseudo code for WebGPU 3DGS rendering

Require: Gaussians Models: $\mathcal{M}_k = \{(\mu_i, s_i, r_i, c_i)\}_{i=1}^{N_k}$; camera (V, P) ; per-model transform M_k

Ensure: Rendered frame

```
/* Pre-pack (only once) */
for all gaussian  $i$  do
   $\Sigma_i \leftarrow \text{CovFromScaleRot}(s_i, r_i)$ 
  store upper( $\Sigma_i$ ),  $\mu_i$  and  $c_i$  as FP16-packed u32 buffers
end for
/* Per-frame */
count  $\leftarrow 0$ ; dispatch  $\leftarrow 0$ 
for all model  $\mathcal{M}_k$  do
  bind ModelParams( $M_k$ , offsets, types, SHdeg, ...)
  dispatch PREPROCESSKERNEL( $\mathcal{M}_k$ )
end for
RADIX SORT(depths, indices, count)
RENDERMESHDEPTHPREPASS
DRAWSPLOTSWITHMESHDEPTH(points2d, indices, count,  $D_{\text{mesh}}$ )
back-to-front
procedure PREPROCESS(idx)
  ( $p, \alpha$ )  $\leftarrow$  read pos/opacity;  $\Sigma^{(6)} \leftarrow$  read upper-cov
   $x_w \leftarrow M_k[\mu; 1]$ ;  $x_c \leftarrow V x_w$ ;  $x_{clip} \leftarrow P x_c$ 
  if frustum-cull fails or  $\alpha < \alpha_{\text{min}}$  then
    return
  end if
  compute 2D ellipse ( $v_1, v_2$ ) and NDC center ( $u, v, z$ )
   $rgba \leftarrow$  evaluate color (raw/SH)
   $k \leftarrow \text{ATOMICADD}(\text{count}, 1)$ 
  write points2d[ $k$ ], depths[ $k$ ], indices[ $k$ ]
end procedure
```

heavy skeletal computations including the forward kinematics of the SMPL-X skeleton and the per-Gaussian LBS operations defined above are encapsulated within the model. The canonical Gaussian attributes ($\hat{\mu}, \hat{\Sigma}$) and skinning weights are baked into the model as initializers (constants). During runtime, the client simply feeds the lightweight SMPL-X parameters (θ, β) into the ONNX runtime. The model then acts as a pre-decoder, outputting the transformed positions and covariances directly to the rasterizer, thereby achieving real-time animation without heavy client-side dependency management.

We further adapt R3Avatar [94] to support high-fidelity novel view rendering of human avatars. In this configuration, we likewise pre-calculate and encapsulate the complex skeletal dynamics and neural deformation logic within the ONNX graph. The client provides a frame index as input. Internally, the ONNX runtime maps this index to the corresponding temporal state, decodes the specific avatar configuration, and outputs the deformed Gaussians directly to the rasterizer.

3.4 WebGPU-based Hybrid Renderer

Visionary renders multiple 3DGS models together with optional mesh assets in a single WebGPU pipeline, and composes them via depth-aware composition. Each Gaussian primitive stores position μ_i , scale s_i , rotation r_i , and appearance c_i (raw RGB or SH). For efficiency, we pre-pack Gaussian attributes into GPU-friendly buffers and execute per-frame screen-space preprocessing and sorting entirely on the GPU.

Pre-pack and FP16 layout. Given a Gaussian parameter unit (μ_i, s_i, r_i, c_i) , s_i and r_i are converted into a symmetric covariance $\Sigma_i \in \mathbb{R}^{3 \times 3}$, and the upper-triangular 6-tuple are stored as $\Sigma_i^{(6)}$. We then cast $(\mu_i, \alpha_i, \Sigma_i^{(6)}, c_i)$ to fp16 and pack every two units into u32 storage to reduce bandwidth.

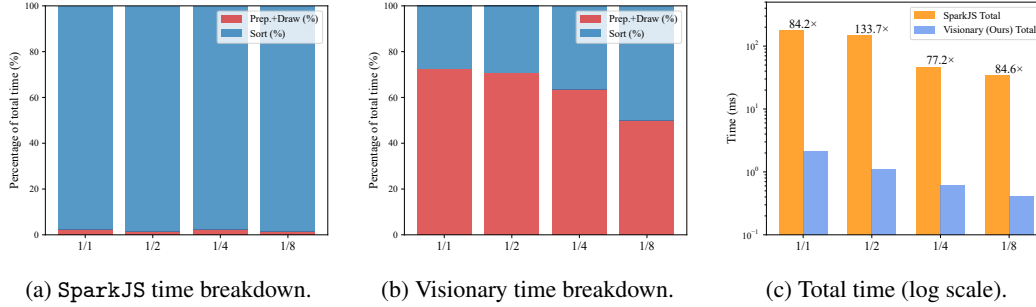


Figure 3: **Runtime comparison.** Experiments are done under identical Gaussian complexity using the classic “bicycle” scene of 3DGS [34] (6M Gaussians at full resolution, and 1/2, 1/4, 1/8 scales). (a): SparkJS shows a dominant CPU sorting cost. (b): Visionary shifts computation to GPU with low and stable overhead. (c): Log-scale comparison shows up to $\sim 100\times$ speed-up over SparkJS.

Per-frame preprocessing. For each loaded model $\mathcal{M}_k = \{(\mu_i, s_i, r_i, c_i)\}_{i=1}^{N_k}$, we dispatch a compute kernel that (i) applies a user-defined affine transformation M_k to \mathcal{M}_k , (ii) transforms its parameter units to camera space and clip space, (iii) performs frustum and opacity culling to remove invalid splats, and (iv) computes the 2D ellipse eigenvectors (v_1, v_2) and NDC center (u, v, z) (written as `Splat`). Valid splats are appended into global buffers via an atomic counter and simultaneously write depth values, *i.e.* the z in NDC space, as keys for sorting in the next step.

GPU sorting and rasterization. After preprocessing, we perform a GPU radix sort [55] over depths and then draw all splats using instanced rasterization. The vertex shader expands each splat into a screen-space quad using (v_1, v_2) , while the fragment shader evaluates the Gaussian weight and outputs pre-multiplied color.

Depth-aware composition with mesh. If a mesh is present, we first rasterize the mesh to obtain a depth buffer D_{mesh} (and optionally its color). During Gaussian rasterization, we keep *depth test enabled but depth write disabled*: Gaussian fragments with $z_{\text{gs}} > D_{\text{mesh}}$ are rejected (occluded by mesh), while visible fragments are alpha-composited in back-to-front order.

3.5 ONNX-based Post-processing

In our ONNX-based post-processing workflow, we export the diffusion denoiser (U-Net [69, 29]) to a Web-friendly ONNX graph. Here, we take EXGS [11] as an example of post processing enhancement and talk about how to export it. Concretely, we load the model and wrap it with a lightweight adapter that standardizes timestep handling, either using a fixed timestep buffer for a specific denoising step or exposing the timestep as a dynamic input. The model is then switched to the evaluation mode and optionally cast to FP16 on the target device for efficient inference.

We next construct shape-correct dummy inputs and optionally enable dynamic axes. The exported ONNX can then run with varying inference shapes. After a sanity-check forward pass, we invoke `torch.onnx.export()` with appropriate input/output names, opset version, and constant folding. The exported model is finally validated via `onnx.checker.check_model()`.

4 Experiments

4.1 Setup

We evaluate Visionary as a web-native renderer that couples per-frame Gaussian generation (ONNX) with high-throughput WebGPU splatting. We focus our evaluation on two aspects: (i) end-to-end rendering efficiency and scalability on static 3DGS assets, and (ii) visual robustness of alpha-composited splatting under challenging interaction patterns (*e.g.*, rapid view changes) and multi-component composition. We compare against representative WebGL-based viewers, including SparkJS and SuperSplat. Unless otherwise stated, all comparisons are conducted using identical 3DGS assets and camera trajectories. Also, we report the runtime of different variants implemented with our

Table 1: **Time analysis.** The sorting process in SparkJS is performed on the CPU. The GPU execution time is obtained using PIX replay, where we first capture a representative frame in PIX and then replay it within PIX to profile performance.

# GS [M]	SparkJS			Visionary (Ours)		
	Sort [ms]	Prep.+Draw [ms]	Total [ms]	Sort [ms]	Prep.+Draw [ms]	Total [ms]
6.062 (1/1)	172.87	4.03	176.90	0.58	1.52	2.09
3.031 (1/2)	143.50	2.25	145.75	0.32	0.77	1.09
1.515 (1/4)	45.27	1.03	46.29	0.22	0.38	0.60
0.758 (1/8)	33.31	0.52	33.82	0.20	0.20	0.40

WebGPU renderer. All experiments are conducted on a workstation equipped with an NVIDIA RTX 4090 GPU and an Intel w5-3435X CPU.

Table 2: **Rendering quality analysis.** Evaluated on MipNeRF360 [7] dataset.

	PSNR \uparrow	SSIM \uparrow	LPIPS \downarrow
SparkJS	27.315	0.825	0.253
Visionary (Ours)	27.867	0.828	0.249

4.2 Runtime and Scalability vs. SparkJS

We first benchmark a standard large-scale static scene: the classic `bicycle` 3DGS asset with ~ 6 M Gaussians at full resolution, and its downscaled variants (1/2, 1/4, 1/8). Figure 3 reports the frame-time breakdown and the end-to-end latency in Table 1. To notice, we measure the GPU execution time using PIX replay, where we first capture a representative frame in PIX and then replay it within PIX to profile performance.

SparkJS is bottlenecked by CPU-side primitive, which dominates the total frame time. In contrast, Visionary moves per-frame preprocessing and global sorting to WebGPU compute, resulting in low and stable overhead across resolutions. Concretely, at full resolution (6.062M Gaussians), SparkJS spends 172.87ms on sorting and 176.90ms total per frame, while Visionary reduces this to 0.58ms sorting and 2.09ms total per frame. Across resolutions, Visionary achieves up to $\sim 135\times$ end-to-end speedup over SparkJS (Figure 3).

4.3 Rendering Quality

Speed improvements should not come at the cost of image quality. On the MipNeRF360 [7] benchmark, Visionary matches (and slightly improves) the rendering quality compared to SparkJS in terms of PSNR, SSIM and LPIPS as in table 2. This slight improvement can be attributed to two design choices: Visionary avoids the aggressive quantization used in SparkJS to preserve more detail while still maintaining interactive speed, and our WebGPU implementation performs 3DGS preprocessing in compute shaders rather than relying on a rasterization-based WebGL pipeline.

4.4 Robustness under Rapid Viewpoint Changes

SparkJS lazy sorting. Besides average frame time, interactive viewers must remain visually stable under fast user input. SparkJS adopts a *lazy sorting* strategy to reduce CPU overhead by reusing a stale ordering and updating it incrementally, which means instead of re-sorting splats every frame in lockstep with rendering, it performs asynchronous updates that are amortized over multiple frames, so the ordering can lag behind the current view. However, when the camera rotates quickly, the depth ordering can change drastically between frames, and the approximate ordering may become invalid. This leads to incorrect alpha compositing and visible artifacts (*e.g.*, popping, streaking, and inconsistent transparency), as shown in Figure 4.



Figure 4: **Artifacts caused by lazy sorting in SparkJS.** When rotating the viewpoint rapidly, the stale/incrementally updated order can become invalid, producing incorrect alpha compositing and visible temporal artifacts. The efficient implementation of Visionary avoids this flaw. The version of SparkJS tested here is the latest available, v0.1.10.

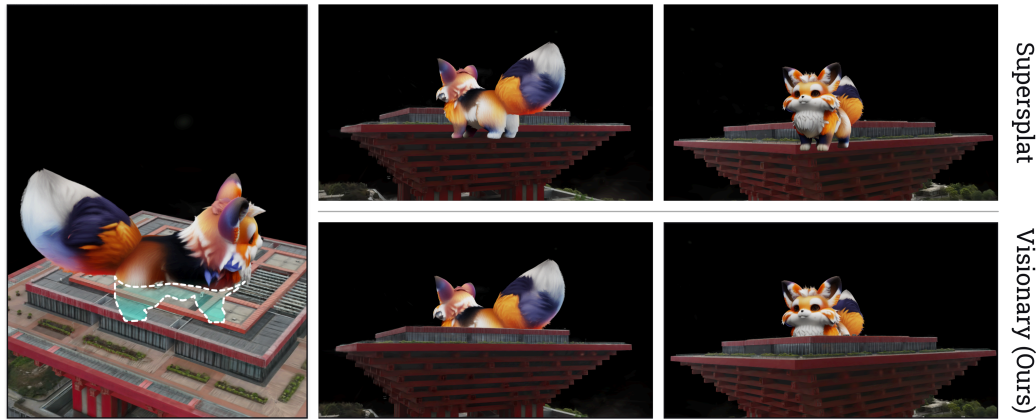


Figure 5: **Wrong visualization caused by local sorting in Supersplat.** Without a global ordering, overlapping Gaussians across partitions may be composited in an incorrect order. Visionary’s efficient global sorting avoids this issue. The version of Supersplat tested here is the latest available, v2.15.1.

Visionary avoids this kind of failure by performing a true *global per-frame sorting* on the GPU for all visible splats. Although sorting is non-trivial, our WebGPU compute implementation keeps the overhead small and stable, and preserves correct back-to-front compositing under fast camera motion.

4.5 Composition Correctness vs. Supersplat

Why global sorting matters? SuperSplat improves performance by avoiding a full global ordering and instead relies on *local sorting* (e.g., sorting within partitions). While efficient, such a strategy is not equivalent to a single global back-to-front ordering. When Gaussians from different partitions overlap substantially, the lack of a global order leads to inconsistent blending between partitions, yielding depth-inconsistent transparency (Figure 5).

Visionary uses a unified global buffer and performs one global sort for *all* valid splats across all loaded models within the same frame, ensuring correct compositing even when multiple 3DGS assets (or 3DGS + mesh) are rendered together.

Table 3: Inference time of MLP-based 3DGS and 4DGS.

	Scaffold-GS [51]		4DGS [79]	
# GS [M]	2.49	4.56	0.03	0.06
Time [ms]	9.29	16.10	4.76	7.93

Table 4: Inference time of Avatar.

	Gauhuman [30]			R ³ -Avatar [94]		
# Instances	1	5	10	1	5	10
# GS [M]	0.04	0.20	0.40	0.02	0.12	0.23
Time [ms]	7.97	28.60	55.63	7.46	27.10	53.35

4.6 Overhead of ONNX-based Gaussian pre-decoding

Finally, we report the runtime feasibility of integrating representative dynamic or structured 3DGS variants through our ONNX-based Gaussian Generator contract. For MLP-based 3DGS (*e.g.*, Scaffold-GS [51]) and deformable 3DGS or 4DGS [79], the per-frame decoding runs in real-time across different scenes as in Table 3. For animatable avatars [30, 64, 94], we observe per-frame inference in the range of 7–8ms depending on the specific model as in Table 4. Note that avatars typically require fewer Gaussians. These results indicate that a single browser-resident pipeline can support both fast rendering and per-frame neural updates.

For 3DGS variants beyond the original 3DGS implementation and diffusion-based post-processing effects, there are currently no other web viewers that support comparable functionality; we therefore refer readers to the accompanying video demos and our online editor for qualitative inspection and interactive exploration.

5 Discussion

5.1 Large World Model & Future

The definition and implementation of world models are still under active debate, with no single absolutely dominant paradigm. Some approaches, such as Marble and FlashWorld [39], generate 3DGS scenes from images or text and emphasize reconstructive, geometrically consistent representations. Others, such as Genie 3 and RTFM, follow a video-generation paradigm that prioritizes creative synthesis and open-ended dynamics. We believe that the next generation of world model renderers should combine the strengths of both paradigms, forming a closed loop between generation and reconstruction. Visionary is designed as an initial step toward this unified framework.

Building on the current architecture, several promising directions can be explored. First, we plan to improve physical interaction by integrating collision detection and further coupling with mesh-based pipelines [26]. Second, we aim to incorporate physics-aware modeling, in which 3DGS representations are combined with methods such as the Material Point Method (MPM) to simulate realistic dynamics [83, 46, 47]. Third, we will investigate spatially grounded 3D agents built on top of multimodal language models [85, 8, 86], enabling reasoning and interaction within complex environments. Finally, Visionary can serve as a bridge to downstream applications by interfacing with vectorized physics simulators, such as Isaac Gym [54], and by integrating relighting [20, 44] and domain adaptation techniques to support Sim-to-Real transfer for embodied AI [17, 32].

5.2 Limitations

WebGPU and ONNX runtimes are still evolving, which may lead to compatibility and stability differences across browsers and operating systems. In addition, current browser security policies impose CPU memory constraints, limiting the size of models that can be executed fully in-browser using off-the-shelf tools. As a result, while small-scale to medium-scale networks can be integrated into the pipeline, some post-processing steps currently remain offline.

6 Conclusion

Visionary addresses several fundamental barriers in neural rendering platforms, including the lack of effective web-native computation, limited extensibility, and heavy system dependencies. By combining a modern, compute-capable graphics API (WebGPU) with a unified ONNX-based integration contract, Visionary enables real-time, in-browser rendering of diverse 3DGS variants in a portable, lightweight, and research-friendly manner, with support for generative post-processing. Beyond serving as a renderer, it acts as a unified carrier for both reconstructive and generative world modeling paradigms, establishing an open and extensible foundation for future advances in spatial intelligence, embodied agents, and interactive 3D environments.

Acknowledgments

This work was partially supported by the Shanghai AI Laboratory. We thank Kang An² and Tianchen Hao² for their contributions to the project during their internships at the Shanghai AI Laboratory.

References

- [1] A. Ajay, Y. Du, A. Gupta, J. Tenenbaum, T. Jaakkola, and P. Agrawal. Is conditional generative modeling all you need for decision-making? *arXiv preprint arXiv:2211.15657*, 2022.
- [2] A. Ali, J. Bai, M. Bala, Y. Balaji, A. Blakeman, T. Cai, J. Cao, T. Cao, E. Cha, Y.-W. Chao, et al. World simulation with video foundation models for physical ai. *arXiv preprint arXiv:2511.00062*, 2025.
- [3] E. Alonso, A. Jelley, V. Micheli, A. Kanervisto, A. J. Storkey, T. Pearce, and F. Fleuret. Diffusion for world modeling: Visual details matter in atari. *Advances in Neural Information Processing Systems*, 37:58757–58791, 2024.
- [4] M. Assran, A. Bardes, D. Fan, Q. Garrido, R. Howes, M. Muckley, A. Rizvi, C. Roberts, K. Sinha, A. Zholus, et al. V-jepa 2: Self-supervised video models enable understanding, prediction and planning. *arXiv preprint arXiv:2506.09985*, 2025.
- [5] J. Bae, S. Kim, Y. Yun, H. Lee, G. Bang, and Y. Uh. Per-gaussian embedding-based deformation for deformable 3d gaussian splatting. In *European Conference on Computer Vision*, pages 321–335. Springer, 2024.
- [6] J. T. Barron, B. Mildenhall, M. Tancik, P. Hedman, R. Martin-Brualla, and P. P. Srinivasan. Mip-nerf: A multiscale representation for anti-aliasing neural radiance fields. In *Proceedings of the IEEE/CVF international conference on computer vision*, pages 5855–5864, 2021.
- [7] J. T. Barron, B. Mildenhall, D. Verbin, P. P. Srinivasan, and P. Hedman. Mip-nerf 360: Unbounded anti-aliased neural radiance fields. In *Proceedings of the IEEE/CVF conference on computer vision and pattern recognition*, pages 5470–5479, 2022.
- [8] E. Brown, A. Ray, R. Krishna, R. Girshick, R. Fergus, and S. Xie. Sims-v: Simulated instruction-tuning for spatial video understanding. *arXiv preprint arXiv:2511.04668*, 2025.
- [9] D. Charatan, S. L. Li, A. Tagliasacchi, and V. Sitzmann. pixelsplat: 3d gaussian splats from image pairs for scalable generalizable 3d reconstruction. In *Proceedings of the IEEE/CVF conference on computer vision and pattern recognition*, pages 19457–19467, 2024.
- [10] D. Chen, H. Li, W. Ye, Y. Wang, W. Xie, S. Zhai, N. Wang, H. Liu, H. Bao, and G. Zhang. Pgsr: Planar-based gaussian splatting for efficient and high-fidelity surface reconstruction. *arXiv preprint arXiv:2406.06521*, 2024.
- [11] J. Chen, X. Ji, Y. Gao, H. Li, Y. Gong, Y. Liu, D. Xu, Z. Zhong, D. Zhang, and X. Sun. Exgs: Extreme 3d gaussian compression with diffusion priors. *arXiv preprint arXiv:2509.24758*, 2025.

- [12] Y. Chen, H. Xu, C. Zheng, B. Zhuang, M. Pollefeys, A. Geiger, T.-J. Cham, and J. Cai. Mvsplat: Efficient 3d gaussian splatting from sparse multi-view images. In *European Conference on Computer Vision*, pages 370–386. Springer, 2024.
- [13] Y. Chen, Y. Zhan, Z. Zhong, W. Wang, X. Sun, Y. Qiao, and Y. Zheng. Within the dynamic context: Inertia-aware 3d human modeling with pose sequence. In *European Conference on Computer Vision*, pages 491–508. Springer, 2024.
- [14] Z. Chen, H.-a. Gao, D. Qu, H. Chi, H. Tang, K. Zhang, and H. Zhao. Alias-free 4d gaussian splatting. *arXiv preprint arXiv:2511.18367*, 2025.
- [15] W. O. Cho, I. Cho, S. Kim, J. Bae, Y. Uh, and S. J. Kim. 4d scaffold gaussian splatting for memory efficient dynamic scene reconstruction. *arXiv preprint arXiv:2411.17044*, 2024.
- [16] E. Decart, Q. McIntyre, S. Campbell, X. Chen, and R. Wachen. Oasis: A universe in a transformer. URL: <https://oasis-model.github.io>, 2024.
- [17] A. Escontrela, J. Kerr, A. Allshire, J. Frey, R. Duan, C. Sferrazza, and P. Abbeel. Gaussgym: An open-source real-to-sim framework for learning locomotion from pixels. *arXiv preprint arXiv:2510.15352*, 2025.
- [18] Z. Fan, K. Wang, K. Wen, Z. Zhu, D. Xu, Z. Wang, et al. Lightgaussian: Unbounded 3d gaussian compression with 15x reduction and 200+ fps. *Advances in neural information processing systems*, 37:140138–140158, 2024.
- [19] S. Fridovich-Keil, A. Yu, M. Tancik, Q. Chen, B. Recht, and A. Kanazawa. Plenoxels: Radiance fields without neural networks. In *Proceedings of the IEEE/CVF conference on computer vision and pattern recognition*, pages 5501–5510, 2022.
- [20] J. Gao, C. Gu, Y. Lin, Z. Li, H. Zhu, X. Cao, L. Zhang, and Y. Yao. Relightable 3d gaussians: Realistic point cloud relighting with brdf decomposition and ray tracing. In *European Conference on Computer Vision*, pages 73–89. Springer, 2024.
- [21] R. Gao, K. Chen, E. Xie, L. Hong, Z. Li, D.-Y. Yeung, and Q. Xu. Magicdrive: Street view generation with diverse 3d geometry control. *arXiv preprint arXiv:2310.02601*, 2023.
- [22] S. Gao, J. Yang, L. Chen, K. Chitta, Y. Qiu, A. Geiger, J. Zhang, and H. Li. Vista: A generalizable driving world model with high fidelity and versatile controllability. *Advances in Neural Information Processing Systems*, 37:91560–91596, 2024.
- [23] Y. Gao, Y. Gong, Y. Liu, L. Jingfeng, Z. Zhong, D. Zhang, Y. Zhang, D. Xu, and X. Sun. Proxy-gs: Efficient 3d gaussian splatting via proxy mesh. *arXiv preprint arXiv:2509.24421*, 2025.
- [24] Y. Gao, H. Li, J. Chen, Z. Zou, Z. Zhong, D. Zhang, X. Sun, and J. Han. Citygs-x: A scalable architecture for efficient and geometrically accurate large-scale scene reconstruction. *arXiv preprint arXiv:2503.23044*, 2025.
- [25] Q. Garrido, M. Assran, N. Ballas, A. Bardes, L. Najman, and Y. LeCun. Learning and leveraging world models in visual representation learning. *arXiv preprint arXiv:2403.00504*, 2024.
- [26] H. Guo, D. Weng, M. Su, Y. Chen, X. Dongye, and C. Xu. Tagsplat: Topology-aware gaussian splatting for dynamic mesh modeling and tracking. *arXiv preprint arXiv:2512.01329*, 2025.
- [27] J. Guo, Y. Ye, T. He, H. Wu, Y. Jiang, T. Pearce, and J. Bian. Mineworld: a real-time and open-source interactive world model on minecraft. *arXiv preprint arXiv:2504.08388*, 2025.
- [28] M. Hassan, S. Stapf, A. Rahimi, P. Rezende, Y. Haghighi, D. Brüggenmann, I. Katircioglu, L. Zhang, X. Chen, S. Saha, et al. Gem: A generalizable ego-vision multimodal world model for fine-grained ego-motion, object dynamics, and scene composition control. In *Proceedings of the Computer Vision and Pattern Recognition Conference*, pages 22404–22415, 2025.
- [29] J. Ho, A. Jain, and P. Abbeel. Denoising diffusion probabilistic models. *Advances in neural information processing systems*, 33:6840–6851, 2020.

- [30] S. Hu, T. Hu, and Z. Liu. Gauhuman: Articulated gaussian splatting from monocular human videos. In *Proceedings of the IEEE/CVF conference on computer vision and pattern recognition*, pages 20418–20431, 2024.
- [31] Y.-H. Huang, Y.-T. Sun, Z. Yang, X. Lyu, Y.-P. Cao, and X. Qi. Sc-gs: Sparse-controlled gaussian splatting for editable dynamic scenes. In *Proceedings of the IEEE/CVF conference on computer vision and pattern recognition*, pages 4220–4230, 2024.
- [32] Y. Jia, G. Wang, Y. Dong, J. Wu, Y. Zeng, H. Lin, Z. Wang, H. Ge, W. Gu, K. Ding, et al. Discovere: Efficient robot simulation in complex high-fidelity environments. *arXiv preprint arXiv:2507.21981*, 2025.
- [33] L. Jiang, Y. Mao, L. Xu, T. Lu, K. Ren, Y. Jin, X. Xu, M. Yu, J. Pang, F. Zhao, et al. Anysplat: Feed-forward 3d gaussian splatting from unconstrained views. *arXiv preprint arXiv:2505.23716*, 2025.
- [34] B. Kerbl, G. Kopanas, T. Leimkühler, and G. Drettakis. 3d gaussian splatting for real-time radiance field rendering. *ACM Trans. Graph.*, 42(4):139–1, 2023.
- [35] B. Kerbl, A. Meuleman, G. Kopanas, M. Wimmer, A. Lanvin, and G. Drettakis. A hierarchical 3d gaussian representation for real-time rendering of very large datasets. *ACM Transactions on Graphics (TOG)*, 43(4):1–15, 2024.
- [36] J. C. Lee, D. Rho, X. Sun, J. H. Ko, and E. Park. Compact 3d gaussian representation for radiance field. In *Proceedings of the IEEE/CVF Conference on Computer Vision and Pattern Recognition*, pages 21719–21728, 2024.
- [37] H. Li, Y. Gao, C. Wu, D. Zhang, Y. Dai, C. Zhao, H. Feng, E. Ding, J. Wang, and J. Han. Ggrt: Towards pose-free generalizable 3d gaussian splatting in real-time. In *European Conference on Computer Vision*, pages 325–341. Springer, 2024.
- [38] R. Li, P. Torr, A. Vedaldi, and T. Jakab. Vmem: Consistent interactive video scene generation with surfel-indexed view memory. *arXiv preprint arXiv:2506.18903*, 2025.
- [39] X. Li, T. Wang, Z. Gu, S. Zhang, C. Guo, and L. Cao. Flashworld: High-quality 3d scene generation within seconds. *arXiv preprint arXiv:2510.13678*, 2025.
- [40] X. Li, Y. Zhang, and X. Ye. Drivingdiffusion: layout-guided multi-view driving scenarios video generation with latent diffusion model. In *European Conference on Computer Vision*, pages 469–485. Springer, 2024.
- [41] Z. Li, Z. Chen, Z. Li, and Y. Xu. Spacetime gaussian feature splatting for real-time dynamic view synthesis. In *Proceedings of the IEEE/CVF Conference on Computer Vision and Pattern Recognition*, pages 8508–8520, 2024.
- [42] Z. Li, Q. Wang, F. Cole, R. Tucker, and N. Snavely. Dynibar: Neural dynamic image-based rendering. In *Proceedings of the IEEE/CVF Conference on Computer Vision and Pattern Recognition*, pages 4273–4284, 2023.
- [43] Z. Li, Z. Zheng, L. Wang, and Y. Liu. Animatable gaussians: Learning pose-dependent gaussian maps for high-fidelity human avatar modeling. In *Proceedings of the IEEE/CVF conference on computer vision and pattern recognition*, pages 19711–19722, 2024.
- [44] Z. Liang, Q. Zhang, Y. Feng, Y. Shan, and K. Jia. Gs-ir: 3d gaussian splatting for inverse rendering. In *Proceedings of the IEEE/CVF Conference on Computer Vision and Pattern Recognition*, pages 21644–21653, 2024.
- [45] J. Lin, Z. Li, X. Tang, J. Liu, S. Liu, J. Liu, Y. Lu, X. Wu, S. Xu, Y. Yan, et al. Vastgaussian: Vast 3d gaussians for large scene reconstruction. *arXiv preprint arXiv:2402.17427*, 2024.
- [46] Y. Lin, C. Lin, J. Xu, and Y. Mu. Omniphysgs: 3d constitutive gaussians for general physics-based dynamics generation. *arXiv preprint arXiv:2501.18982*, 2025.
- [47] I. Liu, H. Su, and X. Wang. Dynamic gaussians mesh: Consistent mesh reconstruction from dynamic scenes. *arXiv preprint arXiv:2404.12379*, 2024.

- [48] Y. Liu, C. Luo, L. Fan, N. Wang, J. Peng, and Z. Zhang. Citygaussian: Real-time high-quality large-scale scene rendering with gaussians. In *European Conference on Computer Vision*, pages 265–282. Springer, 2024.
- [49] Y. Liu, Z. Zhong, Y. Zhan, S. Xu, and X. Sun. Maskgaussian: Adaptive 3d gaussian representation from probabilistic masks. In *Proceedings of the Computer Vision and Pattern Recognition Conference*, pages 681–690, 2025.
- [50] J. Lu, J. Deng, R. Zhu, Y. Liang, W. Yang, T. Zhang, and X. Zhou. Dn-4dgs: Denoised deformable network with temporal-spatial aggregation for dynamic scene rendering. *Advances in Neural Information Processing Systems*, 37:84114–84138, 2024.
- [51] T. Lu, M. Yu, L. Xu, Y. Xiangli, L. Wang, D. Lin, and B. Dai. Scaffold-gs: Structured 3d gaussians for view-adaptive rendering. In *Proceedings of the IEEE/CVF Conference on Computer Vision and Pattern Recognition*, pages 20654–20664, 2024.
- [52] J. Lyu, Z. Li, X. Shi, C. Xu, Y. Wang, and H. Wang. Dywa: Dynamics-adaptive world action model for generalizable non-prehensile manipulation. *arXiv preprint arXiv:2503.16806*, 2025.
- [53] B. Ma, H. Gao, H. Deng, Z. Luo, T. Huang, L. Tang, and X. Wang. You see it, you got it: Learning 3d creation on pose-free videos at scale. In *Proceedings of the Computer Vision and Pattern Recognition Conference*, pages 2016–2029, 2025.
- [54] V. Makoviychuk, L. Wawrzyniak, Y. Guo, M. Lu, K. Storey, M. Macklin, D. Hoeller, N. Rudin, A. Allshire, A. Handa, et al. Isaac gym: High performance gpu-based physics simulation for robot learning. *arXiv preprint arXiv:2108.10470*, 2021.
- [55] P. M. McIlroy, K. Bostic, and M. D. McIlroy. Engineering radix sort. *Computing systems*, 6(1):5–27, 1993.
- [56] B. Mildenhall, P. P. Srinivasan, M. Tancik, J. T. Barron, R. Ramamoorthi, and R. Ng. Nerf: Representing scenes as neural radiance fields for view synthesis. In *ECCV*, 2020.
- [57] T. Müller, A. Evans, C. Schied, and A. Keller. Instant neural graphics primitives with a multiresolution hash encoding. *ACM transactions on graphics (TOG)*, 41(4):1–15, 2022.
- [58] M. Niu, M. Cao, Y. Zhan, Q. Zhu, M. Ma, J. Zhao, Y. Zeng, Z. Zhong, X. Sun, and Y. Zheng. Anicrafter: Customizing realistic human-centric animation via avatar-background conditioning in video diffusion models. *arXiv preprint arXiv:2505.20255*, 2025.
- [59] M. Niu, Y. Zhan, Q. Zhu, Z. Li, W. Wang, Z. Zhong, X. Sun, and Y. Zheng. Bundle adjusted gaussian avatars deblurring. *arXiv preprint arXiv:2411.16758*, 2024.
- [60] G. Pavlakos, V. Choutas, N. Ghorbani, T. Bolkart, A. A. A. Osman, D. Tzionas, and M. J. Black. Expressive body capture: 3D hands, face, and body from a single image. In *Proceedings IEEE Conf. on Computer Vision and Pattern Recognition (CVPR)*, pages 10975–10985, 2019.
- [61] S. Peng, Y. Zhang, Y. Xu, Q. Wang, Q. Shuai, H. Bao, and X. Zhou. Neural body: Implicit neural representations with structured latent codes for novel view synthesis of dynamic humans. In *Proceedings of the IEEE/CVF conference on computer vision and pattern recognition*, pages 9054–9063, 2021.
- [62] A. Pumarola, E. Corona, G. Pons-Moll, and F. Moreno-Noguer. D-nerf: Neural radiance fields for dynamic scenes. In *Proceedings of the IEEE/CVF conference on computer vision and pattern recognition*, pages 10318–10327, 2021.
- [63] Z. Qian, S. Wang, M. Mihajlovic, A. Geiger, and S. Tang. 3dgs-avatar: Animatable avatars via deformable 3d gaussian splatting. In *Proceedings of the IEEE/CVF conference on computer vision and pattern recognition*, pages 5020–5030, 2024.
- [64] L. Qiu, X. Gu, P. Li, Q. Zuo, W. Shen, J. Zhang, K. Qiu, W. Yuan, G. Chen, Z. Dong, et al. Lhm: Large animatable human reconstruction model from a single image in seconds. *arXiv preprint arXiv:2503.10625*, 2025.

- [65] K. Ren, L. Jiang, T. Lu, M. Yu, L. Xu, Z. Ni, and B. Dai. Octree-gs: Towards consistent real-time rendering with lod-structured 3d gaussians. *arXiv preprint arXiv:2403.17898*, 2024.
- [66] X. Ren, Y. Lu, T. Cao, R. Gao, S. Huang, A. Sabour, T. Shen, T. Pfaff, J. Z. Wu, R. Chen, et al. Cosmos-drive-dreams: Scalable synthetic driving data generation with world foundation models. *arXiv preprint arXiv:2506.09042*, 2025.
- [67] X. Ren, T. Shen, J. Huang, H. Ling, Y. Lu, M. Nimier-David, T. Müller, A. Keller, S. Fidler, and J. Gao. Gen3c: 3d-informed world-consistent video generation with precise camera control. In *Proceedings of the Computer Vision and Pattern Recognition Conference*, pages 6121–6132, 2025.
- [68] R. Rombach, A. Blattmann, D. Lorenz, P. Esser, and B. Ommer. High-resolution image synthesis with latent diffusion models. In *Proceedings of the IEEE/CVF conference on computer vision and pattern recognition*, pages 10684–10695, 2022.
- [69] O. Ronneberger, P. Fischer, and T. Brox. U-net: Convolutional networks for biomedical image segmentation. In *International Conference on Medical image computing and computer-assisted intervention*, pages 234–241. Springer, 2015.
- [70] L. Russell, A. Hu, L. Bertoni, G. Fedoseev, J. Shotton, E. Arani, and G. Corrado. Gaia-2: A controllable multi-view generative world model for autonomous driving. *arXiv preprint arXiv:2503.20523*, 2025.
- [71] Sara Fridovich-Keil and Giacomo Meanti, F. R. Warburg, B. Recht, and A. Kanazawa. K-planes: Explicit radiance fields in space, time, and appearance. In *CVPR*, 2023.
- [72] Y. Shang, X. Zhang, Y. Tang, L. Jin, C. Gao, W. Wu, and Y. Li. Roboscape: Physics-informed embodied world model. *arXiv preprint arXiv:2506.23135*, 2025.
- [73] R. Shaw, M. Nazarczuk, J. Song, A. Moreau, S. Catley-Chandar, H. Dharmo, and E. Pérez-Pellitero. Swings: sliding windows for dynamic 3d gaussian splatting. In *European Conference on Computer Vision*, pages 37–54. Springer, 2024.
- [74] M. Tancik, E. Weber, E. Ng, R. Li, B. Yi, T. Wang, A. Kristoffersen, J. Austin, K. Salahi, A. Ahuja, et al. Nerfstudio: A modular framework for neural radiance field development. In *ACM SIGGRAPH 2023 conference proceedings*, pages 1–12, 2023.
- [75] J. Wang, M. Chen, N. Karaev, A. Vedaldi, C. Rupprecht, and D. Novotny. Vggg: Visual geometry grounded transformer. In *Proceedings of the Computer Vision and Pattern Recognition Conference*, pages 5294–5306, 2025.
- [76] X. Wang, Z. Zhu, G. Huang, X. Chen, J. Zhu, and J. Lu. Drivedreamer: Towards real-world-drive world models for autonomous driving. In *European conference on computer vision*, pages 55–72. Springer, 2024.
- [77] Y. Wen, Y. Zhao, Y. Liu, F. Jia, Y. Wang, C. Luo, C. Zhang, T. Wang, X. Sun, and X. Zhang. Panacea: Panoramic and controllable video generation for autonomous driving. In *Proceedings of the IEEE/CVF Conference on Computer Vision and Pattern Recognition*, pages 6902–6912, 2024.
- [78] C.-Y. Weng, B. Curless, P. P. Srinivasan, J. T. Barron, and I. Kemelmacher-Shlizerman. Humannerf: Free-viewpoint rendering of moving people from monocular video. In *Proceedings of the IEEE/CVF conference on computer vision and pattern Recognition*, pages 16210–16220, 2022.
- [79] G. Wu, T. Yi, J. Fang, L. Xie, X. Zhang, W. Wei, W. Liu, Q. Tian, and X. Wang. 4d gaussian splatting for real-time dynamic scene rendering. In *Proceedings of the IEEE/CVF conference on computer vision and pattern recognition*, pages 20310–20320, 2024.
- [80] J. Z. Wu, Y. Zhang, H. Turki, X. Ren, J. Gao, M. Z. Shou, S. Fidler, Z. Gojcic, and H. Ling. Difx3d+: Improving 3d reconstructions with single-step diffusion models. In *Proceedings of the Computer Vision and Pattern Recognition Conference*, pages 26024–26035, 2025.

- [81] T. Wu, S. Yang, R. Po, Y. Xu, Z. Liu, D. Lin, and G. Wetzstein. Video world models with long-term spatial memory. *arXiv preprint arXiv:2506.05284*, 2025.
- [82] Z. Xiao, Y. Lan, Y. Zhou, W. Ouyang, S. Yang, Y. Zeng, and X. Pan. Worldmem: Long-term consistent world simulation with memory. *arXiv preprint arXiv:2504.12369*, 2025.
- [83] T. Xie, Z. Zong, Y. Qiu, X. Li, Y. Feng, Y. Yang, and C. Jiang. Physgaussian: Physics-integrated 3d gaussians for generative dynamics. In *Proceedings of the IEEE/CVF Conference on Computer Vision and Pattern Recognition*, pages 4389–4398, 2024.
- [84] W. Xu, Y. Zhan, Z. Zhong, and X. Sun. Sequential gaussian avatars with hierarchical motion context. In *Proceedings of the IEEE/CVF International Conference on Computer Vision*, pages 13592–13603, 2025.
- [85] J. Yang, S. Yang, A. W. Gupta, R. Han, L. Fei-Fei, and S. Xie. Thinking in space: How multimodal large language models see, remember, and recall spaces. In *Proceedings of the Computer Vision and Pattern Recognition Conference*, pages 10632–10643, 2025.
- [86] S. Yang, J. Yang, P. Huang, E. Brown, Z. Yang, Y. Yu, S. Tong, Z. Zheng, Y. Xu, M. Wang, et al. Cambrian-s: Towards spatial supersensing in video. *arXiv preprint arXiv:2511.04670*, 2025.
- [87] Y. Yang, Y. Zhang, M. Wu, K. Zhang, Y. Zhang, H. Yu, Y. Hu, and B. Wang. Twinmarket: A scalable behavioral and social simulation for financial markets. *arXiv preprint arXiv:2502.01506*, 2025.
- [88] Z. Yang, X. Gao, W. Zhou, S. Jiao, Y. Zhang, and X. Jin. Deformable 3d gaussians for high-fidelity monocular dynamic scene reconstruction. In *Proceedings of the IEEE/CVF conference on computer vision and pattern recognition*, pages 20331–20341, 2024.
- [89] Z. Yang, X. Song, X. Xu, Y. Shi, G. Wang, M. K. Kalra, and P. Yan. Xray2xray: World model from chest x-rays with volumetric context. *arXiv preprint arXiv:2506.19055*, 2025.
- [90] Z. Yang, H. Yang, Z. Pan, and L. Zhang. Real-time photorealistic dynamic scene representation and rendering with 4d gaussian splatting. *arXiv preprint arXiv:2310.10642*, 2023.
- [91] K. Ye, T. Shao, and K. Zhou. When gaussian meets surfel: Ultra-fast high-fidelity radiance field rendering. *ACM Transactions on Graphics (TOG)*, 44(4):1–15, 2025.
- [92] Z. Yu, T. Sattler, and A. Geiger. Gaussian opacity fields: Efficient adaptive surface reconstruction in unbounded scenes. *ACM Transactions on Graphics (ToG)*, 43(6):1–13, 2024.
- [93] Y. Zhan, Z. Li, M. Niu, Z. Zhong, S. Nobuhara, K. Nishino, and Y. Zheng. Kfd-nerf: Rethinking dynamic nerf with kalman filter. In *European Conference on Computer Vision*, pages 1–18. Springer, 2024.
- [94] Y. Zhan, W. Xu, Q. Zhu, M. Niu, M. Ma, Y. Liu, Z. Zhong, X. Sun, and Y. Zheng. R3-avatar: Record and retrieve temporal codebook for reconstructing photorealistic human avatars. *arXiv preprint arXiv:2503.12751*, 2025.
- [95] Y. Zhan, Q. Zhu, M. Niu, M. Ma, J. Zhao, Z. Zhong, X. Sun, Y. Qiao, and Y. Zheng. Towards explicit exoskeleton for the reconstruction of complicated 3d human avatars. In *Proceedings of the IEEE/CVF International Conference on Computer Vision*, pages 14259–14269, 2025.
- [96] B. Zhang, C. Fang, R. Shrestha, Y. Liang, X. Long, and P. Tan. Rade-gs: Rasterizing depth in gaussian splatting. *arXiv preprint arXiv:2406.01467*, 2024.
- [97] K. Zhang, Z. Tang, X. Hu, X. Pan, X. Guo, Y. Liu, J. Huang, L. Yuan, Q. Zhang, X.-X. Long, et al. Epona: Autoregressive diffusion world model for autonomous driving. *arXiv preprint arXiv:2506.24113*, 2025.
- [98] W. Zhang, H. Xiang, Z. Liao, X. Lai, X. Li, and L. Zeng. 2dgs-room: Seed-guided 2d gaussian splatting with geometric constrains for high-fidelity indoor scene reconstruction. *arXiv preprint arXiv:2412.03428*, 2024.

- [99] Y. Zhang, Y. Su, C. Wang, T. Li, Z. Wefers, J. Nirschl, J. Burgess, D. Ding, A. Lozano, E. Lundberg, et al. Cellflux: Simulating cellular morphology changes via flow matching. *arXiv preprint arXiv:2502.09775*, 2025.
- [100] G. Zhao, X. Wang, Z. Zhu, X. Chen, G. Huang, X. Bao, and X. Wang. Drivedreamer-2: Llm-enhanced world models for diverse driving video generation. In *Proceedings of the AAAI Conference on Artificial Intelligence*, volume 39, pages 10412–10420, 2025.
- [101] R. Zheng, J. Wang, S. Reed, J. Bjorck, Y. Fang, F. Hu, J. Jang, K. Kundalia, Z. Lin, L. Magne, et al. Flare: Robot learning with implicit world modeling. *arXiv preprint arXiv:2505.15659*, 2025.
- [102] S. Zhou, Y. Du, J. Chen, Y. Li, D.-Y. Yeung, and C. Gan. Robodreamer: Learning compositional world models for robot imagination. *arXiv preprint arXiv:2404.12377*, 2024.